Dalton Transactions

Accepted Manuscript

This is an *Accepted Manuscript*, which has been through the Royal Society of Chemistry peer review process and has been accepted for publication.

Accepted Manuscripts are published online shortly after acceptance, before technical editing, formatting and proof reading. Using this free service, authors can make their results available to the community, in citable form, before we publish the edited article. We will replace this *Accepted Manuscript* with the edited and formatted *Advance Article* as soon as it is available.

You can find more information about *Accepted Manuscripts* in the Information for Authors.

Please note that technical editing may introduce minor changes to the text and/or graphics, which may alter content. The journal's standard Terms & Conditions and the Ethical guidelines still apply. In no event shall the Royal Society of Chemistry be held responsible for any errors or omissions in this *Accepted Manuscript* or any consequences arising from the use of any information it contains.

ROYAL SOCIETY OF CHEMISTRY

www.rsc.org/dalton

High-pressure synthesis, crystal structure and magnetic properties of $TlCrO_3$ perovskite†

Wei Yi,[a,b] Yoshitaka Matsushita,[c] Yoshio Katsuya,[d] Kazunari Yamaura,[e] Yoshihiro Tsujimoto,[f] Igor A. Presniakov,[g] Alexey V. Sobolev,[g] Yana S. Glazkova,[g] Yuliya O. Lekina,[g] Naohito Tsujii,[h] Shigeki Nimori,[i] Kanji Takehana,[i] Yasutaka Imanaka[i] and Alexei A. Belik[*a]

[a]*International Center for Materials Nanoarchitectonics (WPI-MANA), National Institute for Materials Science (NIMS), 1-1 Namiki, Tsukuba, Ibaraki 305-0044, Japan. E-mail: Alexei.Belik@nims.go.jp*

[b]*Institute of Physics and Beijing National Laboratory for Condensed Matter Physics, Chinese Academy of Sciences, Beijing 100190, China.*

[c]*Materials Analysis Station, NIMS, 1-2-1 Sengen, Tsukuba, Ibaraki 305-0047, Japan*

[d]*Synchrotron X-ray Station at SPring-8, NIMS, Kohto 1-1-1, Sayo-cho, Hyogo 679-5148, Japan.*

[e]*Superconducting Properties Unit, NIMS, 1-1 Namiki, Tsukuba, Ibaraki 305-0044, Japan.*

[f]*Materials Processing Unit, NIMS, 1-2-1 Sengen, Tsukuba, Ibaraki 305-0047, Japan.*

[g]*Department of Chemistry, Lomonosov Moscow State University, Leninskie Gory, 119992 Moscow, Russia.*

[h]*Quantum Beam Unit, NIMS, 1-2-1 Sengen, Tsukuba, Ibaraki 305-0047, Japan.*

[i]*Tsukuba Magnet Laboratory, NIMS, 3-13 Sakura, Tsukuba, Ibaraki 305-0003, Japan.*

† Electronic supplementary information (ESI) available: laboratory XRPD patterns, temperature dependence of the lattice parameters between 5 and 300 K, details of magnetic properties.

Dalton Transactions Accepted Manuscript

Abstract

TlMO$_3$ perovskites (M^{3+} = transition metals) are exceptional members of trivalent perovskite families because of the strong covalency of Tl^{3+}-O bonds. Here we report on the synthesis, crystal structure and properties of $TlCrO_3$ investigated with Mössbauer spectroscopy, specific heat, dc/ac magnetization and dielectric measurements. $TlCrO_3$ perovskite is prepared under high pressure (6 GPa) and high temperature (1500 K) conditions. The crystal structure of $TlCrO_3$ is refined using synchrotron X-ray powder diffraction data: space group *Pnma* (No. 62), Z = 4 and lattice parameters a = 5.40318(1) Å, b = 7.64699(1) Å and c = 5.30196(1) Å at 293 K. No structural phase transitions are found between 5 and 300 K. $TlCrO_3$ crystallizes in the $GdFeO_3$-type structure similar to other members of the perovskite chromite family, ACrO$_3$ (A^{3+} = Sc, In, Y and La-Lu). The unit cell volume and Cr-O-Cr bond angles of $TlCrO_3$ are close to those of $DyCrO_3$; however, the Néel temperature of $TlCrO_3$ ($T_N \approx 89$ K) is much smaller than that of $DyCrO_3$ and close to that of $InCrO_3$. Isothermal magnetization studies show that $TlCrO_3$ is a fully compensated antiferromagnet similar to $ScCrO_3$ and $InCrO_3$, but in contrast with RCrO$_3$ (R^{3+} = Y and La-Lu). ac and dc magnetization measurements with a fine step of 0.2 K reveal the existence of two Néel temperatures with very close values at T_{N2} = 87.0 K and T_{N1} = 89.3 K. Magnetic anomalies near T_{N2} are suppressed by static magnetic fields and by 5 % iron doping.

Dalton Transactions Accepted Manuscript

Introduction

Perovskite-type compounds with the general formula $R^{3+}B^{3+}O_3$, where R^{3+} = Y and La-Lu and B^{3+} = V, Cr, Mn, Fe, Co, Ni and $Ni_{0.5}Mn_{0.5}$, have been attracting a lot of attention for decades. RVO$_3$ compounds have been investigated in connection with different orbital and spin orderings and negative magnetization.[1-3] Some RCrO$_3$ compounds exhibit spin-reorientation transitions, and doped RCrO$_3$ are good oxygen-ion conductors and show sensitivity toward methanol, ethanol, some gases and humidity.[4] RMnO$_3$-based materials exhibit multiferroic properties, colossal magnetoresistance, different charge and orbital orderings, and ferromagnetic (FM), antiferromagnetic (AFM), insulating and metallic properties.[5] RFeO$_3$ compounds have high magnetic ordering temperatures[6,7] and also multiferroic properties.[8] RCoO$_3$ compounds have been investigated a lot because of spin-state transitions of Co^{3+}.[9] RNiO$_3$ compounds are interesting because of charge orderings and metal-insulator transitions.[10] Most of the $R^{3+}B^{3+}O_3$ perovskites crystallize in the GdFeO$_3$-type *Pnma* structure, and monoclinic distortions of the GdFeO$_3$ structure are observed in RNiO$_3$ due to charge disproportionation on Ni^{3+} ions[10] and R_2NiMnO$_6$ due to Ni^{2+} and Mn^{4+} ordering.[11]

If we consider the extended family of $R^{3+}B^{3+}O_3$ perovskites (abbreviated as $A^{3+}B^{3+}O_3$ hereinafter) we will find more peculiarities and interesting behaviours. All members with A^{3+} = Bi show distinct structural and physical properties in comparison with R^{3+} = Y and La-Lu because of the lone electron pair of Bi^{3+} and the covalency of the Bi^{3+}-O bonds.[12] BiCrO$_3$ and BiMnO$_3$ adopt the space group $C2/c$, and BiMnO$_3$ is the only stoichiometric trivalent perovskite manganite with ferromagnetic properties (T_C = 100 K). BiCoO$_3$ has a polar $P4mm$ structure with supertetragonality and high-spin Co^{3+} ions.[13] BiNiO$_3$ has the charge disproportionation on the Bi ions to actually yield $Bi_{0.5}{}^{3+}Bi_{0.5}{}^{5+}Ni^{2+}O_3$ and triclinic symmetry (space group P-1); but the charge distribution restores to the trivalent $Bi^{3+}Ni^{3+}O_3$, and the symmetry to the *Pnma* space group above about 4 GPa at room temperature (RT).[14] BiFeO$_3$ (space group $R3c$)[15] and Bi$_2$NiMnO$_6$ are multiferroics.[16]

There exist a number of perovskite compounds with A^{3+} = In, for example, InCrO$_3$,[17] InRhO$_3$,[17] $(In_{1-y}Mn_y)MnO_3$ ($1/9 \le y \le 1/3$)[18] and In$_2$NiMnO$_6$,[19] whose structural and physical properties have just recently been clarified.[18-21] Interestingly,

Dalton Transactions Accepted Manuscript

even though Sc^{3+} (r_{VIII} = 0.870 Å) is smaller than In^{3+} (r_{VIII} = 0.92 Å),[22] the number of reported perovskites with A^{3+} = Sc is larger than that with A^{3+} = In.[23] They include $ScVO_3$,[24] $ScCrO_3$,[20,25] $ScMnO_3$,[26] $ScRhO_3$,[21] $(Sc_{0.95}Co_{0.05})CoO_3$,[23] Sc_2NiMnO_6[23] and $Sc(Ni,Mn)O_3$;[27] most of them have been prepared just recently for the first time. Peculiarities in perovskites with A^{3+} = Sc and In appear because of the small size of Sc^{3+} and In^{3+} ions and resulting large structural distortions and because of the covalency of the In^{3+}-O bonds.

One can expect peculiarities in perovskites with A^{3+} = Tl[17,28] because of the strong covalency of the Tl^{3+}-O bonds. Detailed structural and physical properties have been reported for $TlFeO_3$,[6,7] $TlNiO_3$[29,30] and just recently for $TlMnO_3$.[31] It was indeed found that the Néel temperatures, T_N, of $TlFeO_3$ and $TlNiO_3$ are much smaller than those of the corresponding $RFeO_3$ and $RNiO_3$ families (R = Y and La-Lu), while the unit cell volumes of $TlFeO_3$ and $TlNiO_3$ are close to those of $DyFeO_3$ and $DyNiO_3$, respectively.[6,29] $TlMnO_3$ was found to crystallize in a triclinically distorted $GdFeO_3$-type structure with space group P-1, and properties of $TlMnO_3$ are distinct from those of all other $AMnO_3$ manganites (A^{3+} = Sc, Y, La-Lu and Bi).[31] For $TlCrO_3$, only lattice parameters but no properties have been reported.[17]

Therefore, in this work, we describe the synthesis, crystal structure and properties of $TlCrO_3$. We find that $TlCrO_3$ has the same peculiarities as those found in $TlFeO_3$[6,7] and $TlNiO_3$,[29,30] namely, T_N of $TlCrO_3$ is much smaller than that of $DyCrO_3$, but the unit cell volume and Cr-O-Cr bond angles of $TlCrO_3$ are close to those of $DyCrO_3$. Isothermal magnetization studies show that $TlCrO_3$ is a fully compensated antiferromagnet similar with $ScCrO_3$ and $InCrO_3$, but in contrast with $RCrO_3$ (R^{3+} = Y and La-Lu). ac and dc magnetization measurements revealed the existence of two Néel temperatures with very close values at T_{N2} = 87.0 K and T_{N1} = 89.3 K.

Experimental

$TlCrO_3$ was prepared from a stoichiometric mixture of Cr_2O_3 (99.9 %) and Tl_2O_3 (99.99 %) taking care because of the high toxicity of thallium and its compounds. The mixture (with the weight of about 0.7 g) was placed in Au capsules and treated at 6 GPa in a belt-type high-pressure apparatus at 1500 K for 2 h (heating rate to the desired temperature was 10 min). After the heat treatment, the samples were quenched to RT, and the pressure was slowly released. The $TlCrO_3$ samples were dark-green

Dalton Transactions Accepted Manuscript

pellets, stable in air. $TlCr_{0.95}{}^{57}Fe_{0.05}O_3$ was prepared using the same method from stoichiometric mixtures of Cr_2O_3, Tl_2O_3 and $^{57}Fe_2O_3$.

X-ray powder diffraction (XRPD) data were collected at RT on a RIGAKU Ultima III diffractometer using CuKα radiation (2θ range of 10–100°, a step width of 0.02°, and a counting time of 2 s/step). $TlCrO_3$ contained trace amounts of Cr_2O_3 impurity (Figure S3 in electronic supplementary information (ESI)). The refined lattice parameters of $TlCr_{0.95}{}^{57}Fe_{0.05}O_3$ at RT were a = 5.4009(1) Å, b = 7.6461(2) Å and c = 5.2991(1) Å. Low-temperature XRPD data of $TlCrO_3$ were measured between 4.8 and 300 K on a RIGAKU SmartLab instrument using CuKα1 radiation (45 kV, 200 mA; 2θ range of 5–120°, a step width of 0.01°, and scan speed of 4 deg/min) and a 4 K cryostat system. No structural phase transitions were detected, and no anomalies in the temperature dependence of the lattice parameters were found at T_N (Figure S4 in ESI); the refined lattice parameters of $TlCrO_3$ at 4.8 K were a = 5.3974(1) Å, b = 7.6426(2) Å and c = 5.2928(1) Å.

Synchrotron XRPD data of $TlCrO_3$ were measured at 293 K on a large Debye-Scherrer camera at the BL15XU beam line of SPring-8.[32,33] The intensity data were collected between 1° and 61.5° at 0.003° intervals in 2θ; the incident beam was monochromatized at λ = 0.65298 Å. The sample was packed into a Lindenmann glass capillary (inner diameter: 0.1 mm), which was rotated during the measurement. The absorption coefficient was also measured, and Rietveld analysis was applied using the RIETAN-2000 program.[34]

dc magnetic susceptibilities (χ = **M/H**) were measured with SQUID magnetometers (Quantum Design, MPMS-1T and MPMS-XL) between 2 and 400 K in different applied magnetic fields under both zero-field-cooled (ZFC) and field-cooled (FC) conditions and using pieces of pellets. FC measurements were performed on cooling (FCC) from high temperatures to 2 K and on warming (FCW) after the FCC measurements. In all ZFC measurements, a sample was rapidly (within 3-5 min) inserted into a magnetometer, which was kept at 10 K; then, temperature was set to 2 K, and finally a measurement magnetic field was applied. Isothermal magnetization measurements (M vs H) were performed between −70 and 70 kOe at 2 K and between −10 and 10 kOe at other temperatures using the ZFC and FC regimes. In the FC regime, a sample was cooled to a desired temperature at 10 kOe from 300 K with the cooling rate of 10 K/min; two branches were measured from 10 kOe to −10 kOe and

Dalton Transactions Accepted Manuscript

from −10 kOe to 10 kOe. High-field M vs H measurements were performed on the NIMS hybrid magnet at 2 K between 0 and 280 kOe. In the ZFC regime, a sample was rapidly inserted into a magnetometer kept at a desired temperature; three branches were measured from 0 Oe to 10 kOe, from 10 kOe to −10 kOe, and from −10 kOe to 10 kOe. Frequency dependent ac susceptibility measurements at different static magnetic fields (H_{dc} = 0, 10, 100, 1000 and 10000 Oe) were performed with a Quantum Design MPMS-1T instrument from 150 to 2 K at frequencies (*f*) of 1.99 and 299.5 Hz and an applied oscillating magnetic field (H_{ac}) of 5 Oe. Specific heat, C_p, was recorded between 2 and 300 K on cooling at 0 and 90 kOe by a pulse relaxation method using a commercial calorimeter (Quantum Design PPMS). Dielectric properties of $TlCrO_3$ were measured using an Agilent E4980A LCR meter between 3 and 300 K in the frequency range of 100 Hz and 2 MHz.

^{57}Fe Mössbauer spectra were recorded at 12 and 300 K using a conventional constant-acceleration spectrometer MS-1104Em in the transmission geometry. A radiation source ^{57}Co(Rh) was kept at RT. All isomer shifts are referred to α-Fe at 300 K. Experimental spectra were processed and analysed using methods of spectral simulations implemented in the SpectrRelax program.[35] We had to use a relatively large ^{57}Fe concentration (5%) because of strong absorption of γ rays by heavy Tl^{3+} cations.

Results

Structural parameters of $TlCrO_3$ are summarized in Table 1, and a picture of the corresponding crystal structure is shown in Figure 1. Experimental, calculated and difference synchrotron XRPD profiles are shown in Figure 2. Our lattice parameters of $TlCrO_3$ (*a* = 5.40318(1) Å, *b* = 7.64699(1) Å and *c* = 5.30196(1) Å) agree very well with the reported values (*a* = 5.405 Å, *b* = 7.647 Å and *c* = 5.302 Å).[17] Table 2 gives the primary bond lengths and bond angles, bond-valence sums (BVS)[36] and a distortion parameter of the CrO_6 octahedron (Δ_d(Cr)). The BVS values of all the cation sites are close to the formal ionic values of +3.

The dc magnetic susceptibilities of $TlCrO_3$ and $TlCr_{0.95}{}^{57}Fe_{0.05}O_3$ are shown on Figure 3a and in Figures S5, S6 and S10-13 of ESI. At small magnetic fields, we

Dalton Transactions Accepted Manuscript

observed a difference between the ZFC and FCC curves below about 89 K for $TlCrO_3$ and 88 K for $TlCr_{0.95}{}^{57}Fe_{0.05}O_3$; the difference is typical for AFM materials with small spin canting. However, the FCC curves were different from those of materials with well-defined weak ferromagnetism, e.g. $YCrO_3$ (Figure S5 of ESI). In $YCrO_3$, FCC curves at small magnetic fields are much larger than ZFC curves, and FCC curves have a tendency to saturate. This fact shows that weak ferromagnetism of $TlCrO_3$ and $TlCr_{0.95}{}^{57}Fe_{0.05}O_3$ is extremely small; it is indeed suppressed above about 500 Oe in $TlCrO_3$ (Figure S6b of ESI) and 100 Oe in $TlCr_{0.95}{}^{57}Fe_{0.05}O_3$. The ZFC and FCC curves almost coincided with each other at 10 kOe; and except for peak-like anomalies at T_N, they were typical for antiferromagnets. Interestingly, the ZFC curves at 10 Oe, 100 Oe and 10 kOe also almost coincided with each other in $TlCrO_3$ (Figure S10 in ESI). The inverse FCC magnetic susceptibilities (at 70 kOe) between 200 and 400 K were fit by the Curie-Weiss equation

$$\chi(T) = \mu^2_{\text{eff}} N(3k_B(T-\theta))^{-1} \qquad (1)$$

where μ_{eff} is effective magnetic moment, N is Avogadro's number, k_B is Boltzmann's constant, and θ is the Weiss constant. The fitting parameters were $\mu_{\text{eff}} = 3.973(8)\mu_B$ and $\theta = -245(2)$ K for $TlCrO_3$ and $\mu_{\text{eff}} = 4.049(6)\mu_B$ and $\theta = -234(2)$ K for $TlCr_{0.95}{}^{57}Fe_{0.05}O_3$. The μ_{eff} values were very close to those of $ScCrO_3$ ($\mu_{\text{eff}} = 3.965\mu_B$), $InCrO_3$ ($\mu_{\text{eff}} = 3.945\mu_B$) and $YCrO_3$ ($\mu_{\text{eff}} = 3.958\mu_B$)[20] and to the localized Cr^{3+} moment of $3.87\mu_B$.

Specific heat of $TlCrO_3$ showed sharp anomalies near $T_N = 89$ K (Figure 3b) indicating the onset of long-range magnetic ordering. The magnetic field of 90 kOe had almost no effect indicating the robustness of the AFM state. The specific heat between 2 and 17 K could be fit by the equation (the insert of Figure 3b)

$$C_p(T) = \gamma T + \beta_1 T^3 + \beta_2 T^5 \qquad (2)$$

where the first term is associated with the electronic contribution, and the second and third terms describe the lattice contribution. The γ coefficient was found to be very small; therefore, γ was fixed at zero. The fitted parameters were $\beta_1 = 0.2238(11)$ $mJmol^{-1}K^{-4}$ and $\beta_2 = 4.92(5)\times10^{-4}$ $mJmol^{-1}K^{-6}$. The β_1 value gives the Debye temperature, $\Theta_D = (234Nk_B/\beta_1)^{1/3}$, of 206 K. A broad peak was observed at 19.6 K on C_p/T^3 vs T curves of $TlCrO_3$, which could originate from the Einstein mode in the lattice contribution to the specific heat because of the presence of heavy Tl^{3+} ions (Figure S14 of ESI).

Dalton Transactions Accepted Manuscript

The M vs H curves of $TlCrO_3$ and $TlCr_{0.95}{}^{57}Fe_{0.05}O_3$ at 2 K are given on Figure 4a; they showed an up-turn deviation from the linear behaviour at magnetic fields higher than about 20 kOe. This fact could indicate an increase of a ferromagnetic contribution and a possible field-induced phase transition above 70 kOe. The M vs H curves of $TlCrO_3$ and $TlCr_{0.95}{}^{57}Fe_{0.05}O_3$ were very close to each other and to those of $ScCrO_3$ and $InCrO_3$.[20] The magnetization of $TlCrO_3$ reached about $0.04\mu_B$ at 2 K and 50 kOe. The M vs H curves were shifted from the origin (a negative exchange bias effect) when they were measured in the FC regime below T_N (Figure 4b). No shifts were found in the ZFC regime below T_N and in the FC regime above T_N. This behaviour was observed in many other materials[3,37] (e.g. $ScCrO_3$ and $InCrO_3$)[23] and attributed to different inhomogeneities, such as, the presence of magnetic impurities, where some spins can be pinned. Despite the detection of extremely weak ferromagnetism on the FCC χ vs T curves at small magnetic fields (Figure 3a), the (ZFC) M vs H curves showed no detectable hysteresis and no remnant magnetization (Figure 4) indicating a fully compensated antiferromagnetic state. To check the existence of field-induced transitions, M vs H curves of $TlCrO_3$ and $ScCrO_3$ were measured up to 280 kOe at 2 K (Figure 5). Field-induced transitions were indeed detected from about 98 kOe in $ScCrO_3$ and 104 kOe in $TlCrO_3$, where the M vs H curves demonstrated changes in the slope. The magnetization of $TlCrO_3$ reached about $0.28\mu_B$ at 2 K and 280 kOe, and that of $ScCrO_3$ - $0.36\mu_B$. The M vs H curves between 200 and 280 kOe followed the following equations: $M = 4.30(9)*10^{-2}\mu_B + 1.127(4)*10^{-6}H(Oe)$ for $ScCrO_3$ and $M = 0.96(11)*10^{-2}\mu_B + 9.70(4)*10^{-7}H(Oe)$ for $TlCrO_3$. It means that the field-induced small canted magnetic moment is larger in $ScCrO_3$ in comparison with $TlCrO_3$. We note that very similar high-field M vs H curves were observed in $BiFeO_3$, where a field-induce transition from about 200 kOe corresponds to the destruction of the cycloid magnetic structure.[15]

The ac susceptibility data of $TlCrO_3$ measured with a step of 0.2 K near T_N showed that there are two transitions with close temperatures at T_{N2} = 87.0 K and T_{N1} = 89.3 K (Figure 6a). The transition at 87.0 K had very sharp peaks (the width of the peaks was about 1 K) on both χ' vs T and χ'' vs T curves; the existence of peaks on the χ'' vs T curves indicates the appearance of a weak ferromagnetic moment. The transition at 89.3 K showed λ-type anomalies on the χ' vs T curves and no anomalies at the χ'' vs T curves. Identical behaviour was found in $ScCrO_3$ with T_{N2} = 68.6 K and T_{N1} =

Dalton Transactions Accepted Manuscript

73.0 K.[20] Sharp anomalies at T_{N2} on both χ' vs T and χ'' vs T curves were completely suppressed in $TlCr_{0.95}{}^{57}Fe_{0.05}O_3$, that is, by doping; and this compound showed only λ-type anomalies on the χ' vs T curves at T_N = 87.5 K (Figure S7 of ESI). Sharp anomalies at T_{N2} on both χ' vs T and χ'' vs T curves in $TlCrO_3$ were also suppressed by a static magnetic field (Figure 7a); at fields above 100 Oe, no anomalies can be detected on T_{N2}. On the other hand, a static magnetic field of even 10 kOe had no effects on other parts of the χ' vs T and χ'' vs T curves of $TlCrO_3$ and $TlCr_{0.95}{}^{57}Fe_{0.05}O_3$ (Figure S7 of ESI).

After finding the existence of two Néel temperatures at T_{N2} = 87.0 K and T_{N1} = 89.3 K by ac susceptibility measurements, dc magnetic susceptibility measurements were repeated with a fine step of 0.2 K near T_N (Figures 7b and 8). With the 0.2 K step, dc data also revealed the existence of two peaks on the ZFC curves and two steps on the FCC and FCW curves. dc magnetic anomalies near T_{N2} = 87.0 K were strongly suppressed by a magnetic field. It should be noted that no signs of a double transition near T_N were detected with a measurement step of 1 K (Figure S12 of ESI).

Dielectric measurements showed a very small kink on the dielectric constant of $TlCrO_3$ at T_N (Figure S15 of ESI) similar to the dielectric data of $ScCrO_3$ and $InCrO_3$.[20] The kink in $TlCrO_3$ was observed at frequencies of 200 kHz-2 MHz; at low frequencies, strong dielectric relaxation appeared that masked the anomaly at T_N. The dielectric relaxation appeared at the intermediate temperatures of 90-160 K and at low temperatures of 5-30 K; the similar behaviour was also found in $ScCrO_3$.[20] We note that the dielectric constant of $TlCrO_3$ exhibited a much stronger kink at about 45 K (at 2 MHz); however, that kink was strongly frequency-dependent and coincided with the dielectric relaxation processes, therefore, it is believed to be extrinsic.

Mössbauer spectra of $TlCr_{0.95}{}^{57}Fe_{0.05}O_3$ recorded at $T > T_N$ consisted of a symmetric quadrupole doublet (Figure 9a) with the isomer shift (δ_{300K} = 0.36(1) mm/s) corresponding to the high spin Fe^{3+} ions in the octahedral oxygen coordination.[38] Full width at half maximum (W_{300K} = 0.31(1) mm/s) of the doublet was close to the instrumental resolution (0.28(1) mm/s for α-Fe_2O_3) giving evidence for one crystallographic site for Fe^{3+} ions in agreement with the crystal structure. The quadrupole splitting of the doublet (Δ_{300K} = 0.46(1) mm/s) was in good agreement with Δ_{623K} = 0.47(2) mm/s in $TlFeO_3$.[6] The electric field gradient (EFG) at the ^{57}Fe nuclei in electronically isotropic Fe^{3+}(d^5, $^6A_{1g}$) ions originates from the distortion of

Dalton Transactions Accepted Manuscript

their crystal environment (a lattice contribution). Our calculations of the EFG tensor[6] using the crystal data for $TlCrO_3$ showed that, in addition to a monopole lattice contribution, a dipole contribution has a large weight coming from the induced electric dipole moment of oxygen O^{2-} anions that depends on oxygen dipole polarizability (α_O). The best agreement between the theoretical and experimental values of the quadrupole splitting was obtained for the polarizability of $\alpha_O \approx 1.1$ Å^3 (using formal charges $Z_{Tl} = +3$, $Z_{Cr} = +3$ and $Z_O = -2$). The obtained high value of α_O agrees well with the data for other oxides ($\alpha_O = 0.5$-1.5 Å^3).[39]

Mössbauer spectra recorded at $T < T_N$ (Figure 9b) consisted of hyperfine Zeeman structures reflecting combined electric and magnetic hyperfine interactions. The spectra could be well described as a superposition of two sextets, Fe1 and Fe2, having very different partial contributions ($I_{Fe1} \approx 83\%$ and $I_{Fe2} \approx 17\%$ at 12 K). The most intense Fe1 sextet with the saturated hyperfine field (at $T \rightarrow 0$ K) on ^{57}Fe nuclei of $H_{hf1}(0) = 497(1)$ kOe can be assigned to Fe^{3+} ions antiferromagnetically coupled with the six nearest Cr^{3+} neighbors ($6Cr^{3+}$; $0Fe^{3+}$). The second Fe2 sextet with $H_{hf2}(0) = 455(2)$ kOe can be assigned to Fe^{3+} ions for which one of the six nearest Cr^{3+} neighbors is replaced by an Fe^{3+} cation resulting in the ($5Cr^{3+}$; $1Fe^{3+}$) local surrounding. The partial contribution ($I_{Fe2} \approx 17\%$) of the Fe2 sextet is in agreement with the expected one from the binomial formula (~22 %).

Discussion

The unit cell volume of $TlCrO_3$ ($V = 219.1$ Å^3) is close to that of $DyCrO_3$ ($V = 219.4$ Å^3) similar to the pairs of $TlFeO_3$/$DyFeO_3$ (225.7 Å^3/226.3 Å^3),[6,7] $TlNiO_3$/$DyNiO_3$ (213.3 Å^3/213.4 Å^3),[29,30] $TlMnO_3$/$DyMnO_3$ (227.2 Å^3/227.2 Å^3)[31] and $TlCoO_3$/$DyCoO_3$ (205.79 Å^3/206.47 Å^3; $a = 5.3000(2)$ Å, $b = 7.4519(3)$ Å and $c = 5.2106(2)$ Å for $TlCoO_3$). This fact suggests a revision (proposed in Ref. 29) of the Shannon ionic radius of Tl^{3+}, which is currently close to that of Lu^{3+},[22] to be similar to Dy^{3+}. The Cr-O-Cr bond angles of $TlCrO_3$ (144.18° and 145.91°) are also close to those of $DyCrO_3$ (143.71° and 146.93°: experimental data from neutron diffraction).[40] However, we should mention that the available Cr-O-Cr bond angles of $RCrO_3$ show large variations even for the same composition, for example, 147.8° and 148.8° for $YCrO_3$ (XRPD),[41] 145.6° and 146.3° for $YCrO_3$ (neutron),[42] 145.9° and 148.2° for $HoCrO_3$ (XPRD),[41] 144.3° and 147.7° for $ErCrO_3$ (neutron),[43] 143.3° and 146.7° for

Dalton Transactions Accepted Manuscript

$ErCrO_3$ (XPRD),[44] 140.3° and 145.3° for $TmCrO_3$ (XPRD),[45] 147.5° and 148.0° for $DyCrO_3$ (neutron).[46] Theoretical studies predicted the average Cr-O-Cr bond angle of $DyCrO_3$ to be about 145.5°.[47] Systematic studies of $RCrO_3$ by neutron powder diffraction gave about 148° for $DyCrO_3$,[48] and the average Cr-O-Cr angle of $TlCrO_3$ is close to that of $YbCrO_3$ based on the results of Ref. 48.

Independent of the Tl^{3+} size used ($r_{VIII}(Tl^{3+})$ = 0.98 Å[22] or $r_{VIII}(Tl^{3+}) = r_{VIII}(Dy^{3+})$ = 1.027 Å) the unit cell parameters of $TlCrO_3$ show significant deviations from the general trends of the $ACrO_3$ (A = Sc, Y and La-Lu) family, namely, the b and c parameters are larger than expected, and the a parameter is smaller (Figure 10). The same deviations were observed in $InCrO_3$.[23] Such peculiarities of $InCrO_3$ and $TlCrO_3$ could originate from the strong covalency of the In^{3+}-O and Tl^{3+}-O bonds.

In the $ACrO_3$ (A = Sc, In, Y and La-Lu) family, the Néel temperature (T_N) monotonically decreases with decreasing the radius of the A^{3+} ions from T_N = 288 K for $LaCrO_3$ to T_N = 112 K for $LuCrO_3$,[4,20] T_N = 93 K for $InCrO_3$[20] and T_N = 73 K for $ScCrO_3$.[20] It is well known that the B-O-B bond angle (ϑ), which is reduced from 180^0 due to cooperative rotations of BO_6 octahedra in orthorhombic perovskites, is a major factor that governs the evolution of the superexchange coupling parameter, $J \propto \cos^2\vartheta$, since $T_N = 4S(S+1)J/k_B$ in the mean-field theory approximation.[48] The evolution of T_N with the Cr-O-Cr superexchange angle (ϑ) for $ACrO_3$ is presented in Figure 11. T_N of $TlCrO_3$ is smaller than even that of $InCrO_3$. From this point of view, $TlCrO_3$ is similar with $TlFeO_3$ (T_N = 560 K) and $TlNiO_3$ (T_N = 105 K), whose T_N's are significantly smaller than those of $LuFeO_3$ (T_N = 625 K) and $LuNiO_3$ (T_N = 130 K), respectively.[6,29] But T_N of $TlMnO_3$ (T_N = 92 K) having a different structural distortion (space group P-1) is close to that of the lighter rare earth manganite $PrMnO_3$ (T_N = 100 K).[31] For $AFeO_3$ (A = Tl and Pr-Lu), a correlation was found between T_N and the lattice parameter ratio, $2^{-1/2}b/c$ (in the $Pnma$ setting); $TlFeO_3$ has the significantly lower T_N and $2^{-1/2}b/c$ values in comparison with $RFeO_3$ (R = Pr-Lu).[6,7] However, we could not find such a correlation in $ACrO_3$ (A = Sc, In, Tl, Y and La-Lu): the $2^{-1/2}b/c$ ratio of $TlCrO_3$ (1.020) is close to that of $LuCrO_3$ (1.021).

In addition to the smaller T_N of $TlCrO_3$ in comparison with those of $RCrO_3$, we find an abnormally low value of the hyperfine magnetic field at the ^{57}Fe nuclei in $TlCr_{0.95}Fe_{0.05}O_3$. Figure 11 shows the experimental angular dependences of the saturated hyperfine magnetic fields at ^{57}Fe nuclei, $H_{hf}(\vartheta)$, for $RCr_{0.99}Fe_{0.01}O_3$ (with R

Dalton Transactions Accepted Manuscript

= La, Y and Lu) and $TlCr_{0.95}Fe_{0.05}O_3$.[49] For $RCr_{0.99}Fe_{0.01}O_3$, the H_{hf} values decrease with increasing the average Cr-O-Cr bond angle. This behaviour is due to a super-transferred hyperfine field (H_{STHF}) resulting from a spin transfer from neighbouring 3*d* orbitals of the Cr^{3+} cations via oxygen 2*p* orbitals into *n*s (*n* = 1 - 4) orbitals of central Fe^{3+} cation.[50] The H_{STHF} contribution is sensitive to the ϑ angle in the Fe-O-Cr pathways: $H_{STHF} = H_\sigma \cos^2\vartheta + H_\pi \sin^2\vartheta$, ($H_\sigma$ and H_π are parameters representing the spin-transfer via the σ and π *B*-O bonds in the Fe-O-Cr pathways, respectively).[49,50] The $H_{hf}(0)$ value for $TlCr_{0.95}Fe_{0.05}O_3$ shows a noticeable deviation from the linear dependence $H_{hf}(\vartheta) \propto \cos^2\vartheta$ found in Ref. 49. We suggested that a possible reason for this effect is the indirect influence of Tl^{3+} cations on the parameters of the Cr-O and Fe-O chemical bonds.[7] As Tl^{3+} cations have high polarizability and rather high electron affinity,[39] we assumed that the inductive redistribution within the Tl←O←(Cr,Fe) chains leads to weakening of Cr-O and Fe-O bonds (decrease in the H_π parameter) and, therefore, to decrease in the experimental $H_{hf}(0)$ values for $TlCr_{0.95}Fe_{0.05}O_3$.

The size of Tl^{3+} is within the range of that of the rare-earth cations. Nevertheless, magnetic properties of $TlCrO_3$ are different from those of $RCrO_3$ (*R* = Y and La-Lu) and very close to those of $ScCrO_3$ with the smallest (reported so far) cation at the *A* site. $RCrO_3$ compounds exhibit well-defined weak-ferromagnetic properties because of spin canting of the overall G-type antiferromagnetic structure.[4,20,41,43,44] M vs H curves of $ScCrO_3$,[20] $InCrO_3$ and $TlCrO_3$ (Figures 4 and 5) show that they are fully compensated antiferromagnets without spin canting. This property is quite unexpected considering that all $ACrO_3$ compounds with *A* = Sc, In, Tl, Y and Lu-La are isostructural with each other, and the symmetry should allow spin canting.[47] Spin canting first appears at T_N in $TlCrO_3$ (Figure 3a) as expected, but then it is suppressed. There are some analogies in the M vs H and χ vs *T* curves of $TlCrO_3$ and $BiFeO_3$ (Figure S13 of ESI). The latter one has the short-range G-type antiferromagnetic ordering with spin canting, but the overall magnetic structure has no net moment because of an incommensurate spin cycloid structure with a very long period.[15] dc susceptibility curves of $TlCrO_3$ and $BiFeO_3$ at larger magnetic fields exhibit strong peaks at T_N (Figure S13 of ESI), but then they start to decrease (in $BiFeO_3$, because of the cycloid structure with zero net magnetization). The M vs H curves of $TlCrO_3$ and $BiFeO_3$ demonstrate similar field-induced transitions (in $BiFeO_3$, due to the

Dalton Transactions Accepted Manuscript

destruction of the cycloid structure). Non-trivial magnetic structures of $ScCrO_3$, $InCrO_3$ and $TlCrO_3$ could be at the origin of their different properties in comparison with $RCrO_3$; this idea needs confirmation with neutron diffraction. Therefore, $TlCrO_3$ perovskite has many peculiarities in comparison with $RCrO_3$ (R = Y and La-Lu), originating from the strong covalency of the Tl^{3+}-O bonds.

Conclusion

In conclusion, we prepared $TlCrO_3$ perovskite under high pressure (6 GPa) and high temperature (1500 K) conditions. Structural properties were investigated between 5 and 300 K. We found the existence of two Néel temperatures with very close values at T_{N2} = 87.0 K and T_{N1} = 89.3 K. The transition at T_{N2} is very sensitive to static magnetic fields and different perturbations, such as, small iron doping. Magnetic and dielectric properties of $TlCrO_3$ are very close to those of $ScCrO_3$ despite different sizes of Tl^{3+} and Sc^{3+} cations and different nature of Tl^{3+}-O and Sc^{3+}-O bonds. The absence of spin canting suggests a non-trivial magnetic structure in $TlCrO_3$. $TlCrO_3$ has many peculiarities in comparison with $RCrO_3$ (R = Y and La-Lu).

Acknowledgements

This work was supported by World Premier International Research Center Initiative (WPI Initiative, MEXT, Japan), the Japan Society for the Promotion of Science (JSPS) through its "Funding Program for World-Leading Innovative R&D on Science and Technology (FIRST Program)" and a JSPS Grant-in-Aid for Scientific Research (25289233). The synchrotron radiation experiments were performed at the SPring-8 with the approval of the Japan Synchrotron Radiation Research Institute (Proposal Number: 2014A4504). We thank Dr. J.-S. Zhou for providing numerical data of the average Cr-O-Cr bond angles from Ref. 48.

Dalton Transactions Accepted Manuscript

References

1. J. Fujioka, T. Yasue, S. Miyasaka, Y. Yamasaki, T. Arima, H. Sagayama, T. Inami, K. Ishii and Y. Tokura, *Phys. Rev. B,* 2010, **82**, 144425.
2. Y. Ren, T. T. M. Palstra, D. I. Khomskii, E. Pellegrin, A. A. Nugroho, A. A. Menovsky and G. A. Sawatzky, *Nature*, 1998, **396**, 441-444.
3. A. A. Belik, *Inorg. Chem.,* 2013, **52**, 8529-8539.
4. K. Sardar, M. R. Lees, R. J. Kashtiban, J. Sloan and R. I. Walton, *Chem. Mater.,* 2011, **23**, 48-56.
5. N. Izyumskaya, Ya. Alivov and H. Morkoc, *Crit. Rev. Solid State Mat. Sci.*, 2009, **34**, 89-179.
6. S. J. Kim, G. Demazeau, I. Presniakov and J. H. Choy, *J. Solid State Chem.*, 2001, **161**, 197-204.
7. I. A. Presniakov, A. V. Sobolev, A. V. Baranov, G. Demazeau and V. S. Rusakov, *J. Phys.: Condens. Matter*, 2006, **18**, 8943-8959.
8. Y. Tokunaga, N. Furukawa, H. Sakai, Y. Taguchi, T. Arima and Y. Tokura, *Nature Mater.*, 2009, **8**, 558-562.
9. M. Tachibana, T.Yoshida, H. Kawaji, T. Atake and E.Takayama-Muromachi, *Phys. Rev. B*, 2008, **77**, 094402.
10. M. L. Medarde, *J. Phys.: Condens. Matter,* 1997, **9**, 1679-1707.
11. R. J. Booth, R. Fillman, H. Whitaker, A. Nag, R. M. Tiwari, K. V. Ramanujachary, J. Gopalakrishnan and S. E. Lofland, *Mater. Res. Bull.*, 2009, **44**, 1559-1564.
12. A. A. Belik, *J. Solid State Chem.*, 2012, **195**, 32-40.
13. A. A. Belik, S. Iikubo, K. Kodama, N. Igawa, S. Shamoto, S. Niitaka, M. Azuma, Y. Shimakawa, M. Takano, F. Izumi and E. Takayama-Muromachi, *Chem. Mater.*, 2006, **18**, 798-803.
14. M. Azuma, S. Carlsson, J. Rodgers, M. G. Tucker, M. Tsujimoto, S. Ishiwata, S. Isoda, Y. Shimakawa, M. Takano and J. P. Attfield, *J. Am. Chem. Soc.*, 2007, **129**, 14433-14436.
15. G. Catalan and J. F. Scott, *Adv. Mater.*, 2009, **21**, 2463-2485.
16. M. Azuma, K. Takata, T. Saito, S. Ishiwata, Y, Shimakawa and M. Takano, *J. Am. Chem. Soc.*, 2005, **127**, 8889-8892.
17. R. D. Shannon, *Inorg. Chem.*, 1967, **6**, 1474-1478.
18. A. A. Belik, T. Furubayashi, Y. Matsushita, M. Tanaka, S. Hishita and E. Takayama-Muromachi, *Angew. Chem. Int. Ed.*, 2009, **48**, 6117-6120.
19. W. Yi, Q. Liang, Y. Matsushita, M. Tanaka and A. A. Belik, *Inorg. Chem.*, 2013, **52**, 14108-14115.
20. A. A. Belik, Y. Matsushita, M. Tanaka and E. Takayama-Muromachi, *Chem. Mater.*, 2012, **24**, 2197-2203.
21. A. A. Belik, Y. Matsushita, M. Tanaka, E. Takayama-Muromachi, *Inorg. Chem.*, 2013, **52**, 12005-12011.
22. R. D. Shannon, *Acta Crystallogr., Sec. A* 1976, **32**, 751-767.
23. A. A. Belik and W. Yi, *J. Phys.: Condens. Matter*, 2014, **26**, 163201.
24. E. Castillo-Martinez, M. Bieringer, S. P. Shafi, L. M. D. Cranswick and M. A. Alario-Franco, *J. Am. Chem. Soc.*, 2011, **133**, 8552-8563.
25. J. H. Park and J. B. Parise, *Mater. Res. Bull.*, 1997, **32**, 1617-1624.
26. H. Y. Chen, T. Yu, P. Gao, J. M. Bai, J. Tao, T. A. Tyson, L. Wang and R. Lalancette, *Inorg. Chem.*, 2013, **52**, 9692-9697.
27. C. I. Thomas, M. R. Suchomel, G. V. Duong, A. M. Fogg, J. B. Claridge and M. J. Rosseinsky, *Phil. Trans. R. Soc. A,* 2014, **372**, 20130012.

Dalton Transactions Accepted Manuscript

28. A. S. Viskov, E. V. Zubova, K. P. Burdina and Yu. N. Venevtsev, *Sov. Phys. Crystallogr.*, 1971, **15**, 932-934. (*Kristallografiya,* 1970, **15**, 1071-1073 (in Russian)).
29. S. J. Kim, G. Demazeau, J. A. Alonso and J. H. Choy, *J. Mater. Chem.*, 2001, **11**, 487-492.
30. S. J. Kim, M. J. Martinez-Lope, M. T. Fernandez-Diaz, J. A. Alonso, I. Presniakov and G. Demazeau, *Chem. Mater.*, 2002, **14**, 4926-4932.
31. W. Yi, Y. Kumagai, N. A. Spaldin, Y. Matsushita, A. Sato, I. A. Presniakov, A. V. Sobolev, Y. S. Glazkova and A. A. Belik, *Inorg. Chem.*, 2014, **53**, 9800-9808.
32. M. Tanaka, Y. Katsuya and A. Yamamoto, *Rev. Sci. Instrum.*, 2008, **79**, 075106.
33. M. Tanaka, Y. Katsuya, Y. Matsushita and O. Sakata, *J. Ceram. Soc. Jpn.*, 2013, **121**, 287.
34. F. Izumi and T. Ikeda, *Mater. Sci. Forum***,** 2000, **321-324**, 198-203.
35. M. E. Matsnev and V. S. Rusakov, *AIP Conf. Proc.*, 2012, **1489**, 178-185.
36. N. E. Brese and M. O'Keeffe, *Acta Crystallogr., Sec. B* 1991, **47**, 192-197.
37. A. A. Belik, *J. Phys. Soc. Jpn.*, 2014, **83**, 074703.
38. F. Menil, *J. Phys. Chem. Solids*, 1985, **46**, 763-789.
39. R. D. Shannon and R. X. Fischer, *Phys. Rev. B*, 2006, **73,** 235111.
40. B. V. Laar and J. B. A. A. Elemans, *J. Phys.*, 1971, **32**, 301-304.
41. B. Tiwari, M. K. Surendra and M. S. R. R. Rao, *J. Phys.: Condens. Matter*, 2013, **25**, 216004.
42. K. Ramesha, A. Llobet, Th. Proffen, S. R. Serrao and C. N. R. Rao, *J. Phys.: Condens. Matter*, 2007, **19**, 102202.
43. E. F. Bertaut and J. Mareschal, *Solid State Commun.*, 1967, **5**, 93-97.
44. J. Prado-Gonjal, R. Schmidt, D. Avila, U. Amador and E. Moran, *J. Europ. Ceram. Soc.*, 2012, **32**, 611-618.
45. K. Yoshii, *Mater. Res. Bull.*, 2012, **47**, 3243-3248.
46. E. F. Bertaut and J. Mareschal, *J. Phys.*, 1968, **29**, 67-73.
47. H. J. Zhao, W. Ren, X. M. Chen and L. Bellaiche, *J. Phys.: Condens. Matter*, 2013, **25**, 385604.
48. J.-S. Zhou, J. A. Alonso, V. Pomjakushin, J. B. Goodenough, Y. Ren, J.-Q. Yan and J.-G. Cheng, *Phys. Rev. B*, 2010, **81,** 214115.
49. A. S. Moskvin, N. S. Ovanesyan and V. A. Trukhtanov, *Hyperfine Interact.*, 1975, **1**, 265-281.
50. A. Sawatzky and F. Van Der Woude, *J. Phys*., 1974, **35**, 6-47.

Dalton Transactions Accepted Manuscript

Table 1. Structure Parameters of $TlCrO_3$ at Room Temperature.

Site	WP	*x*	*y*	*z*	*B* (Å^2)
Tl	4*c*	0.04617(3)	0.25	0.98732(5)	0.390(4)
Cr	4*b*	0	0	0.5	0.416(12)
O1	4*c*	0.4504(7)	0.25	0.1050(5)	0.28(5)
O2	8*d*	0.3009(5)	0.0558(3)	0.6969(4)	0.33(5)

WP: Wyckoff position. The occupation factor of all sites is unity.
Space group *Pnma* (No 62); $Z = 4$; $a = 5.40318(1)$ Å, $b = 7.64699(1)$ Å, $c = 5.30196(1)$ Å, and $V = 219.0668(3)$ Å^3; $\rho_{cal} = 9.229$ g/cm^3.
$R_{wp} = 1.61$ % ($S = 1.51$), $R_p = 1.22$ %, $R_B = 3.50$ %, and $R_F = 2.73$ %.
The weight fraction of Cr_2O_3 is 0.8 %.

Table 2. Selected Bond Lengths (l (Å) < 3.1 Å), Bond Angles (deg), Bond Valence Sums, BVS, and Distortion Parameters of CrO_6, Δ, in $TlCrO_3$ [a]

Tl–O2	2.217(2) ×2	Cr–O2	1.979(3) ×2
Tl–O1	2.222(3)	Cr–O2	1.980(3) ×2
Tl–O1	2.272(3)	Cr–O1	2.009(1) ×2
Tl–O2	2.544(2) ×2	BVS(Cr^{3+})	2.93
Tl–O2	2.718(2) ×2	Δ(Cr–O)	0.49×10^{-4}
BVS(Tl^{3+})	2.91	Cr–O1–Cr	144.18(5)
		Cr–O2–Cr	145.91(5) ×2

[a] BVS = $\sum_{i=1}^{N} v_i$, $v_i = \exp[(R_0 - l_i)/B]$, N is the coordination number, $B = 0.37$, $R_0(Tl^{3+}) = 2.003$ and $R_0(Cr^{3+}) = 1.724$.

Dalton Transactions Accepted Manuscript

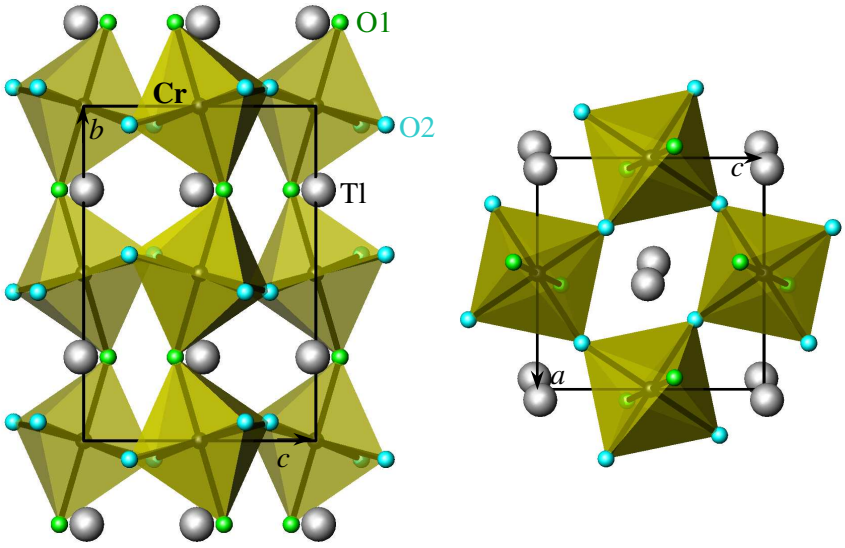

Figure 1. Projections of the crystal structure of $TlCrO_3$ along different directions.

Dalton Transactions Accepted Manuscript

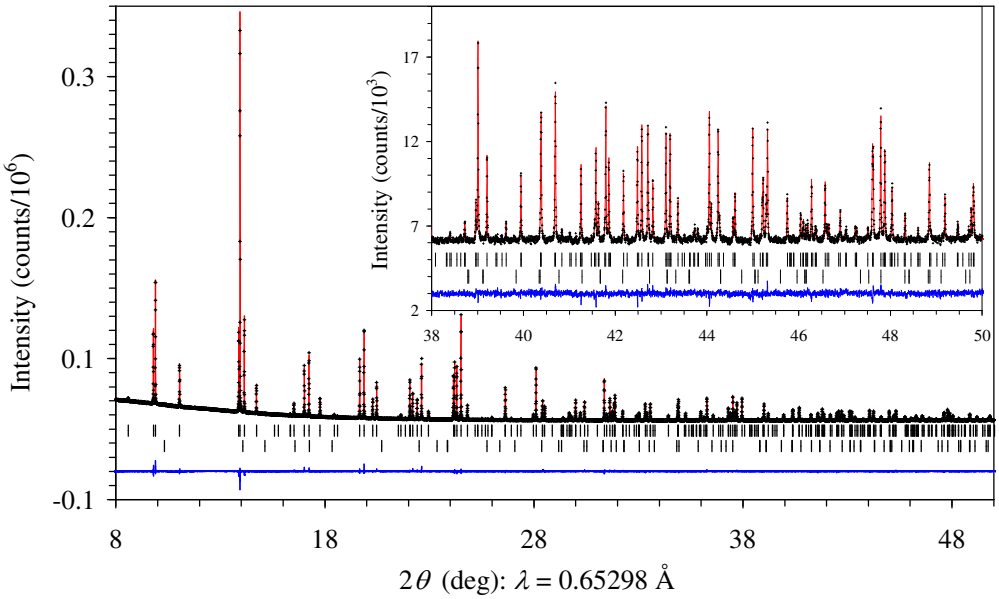

Figure 2. Portions (8-50°) of experimental, calculated and difference synchrotron XRPD diffraction patterns for $TlCrO_3$. The bars show possible Bragg reflection positions for $TlCrO_3$ and Cr_2O_3 impurity (0.8 weight %) (from top to bottom). The insert shows an enlarged fragment.

Dalton Transactions Accepted Manuscript

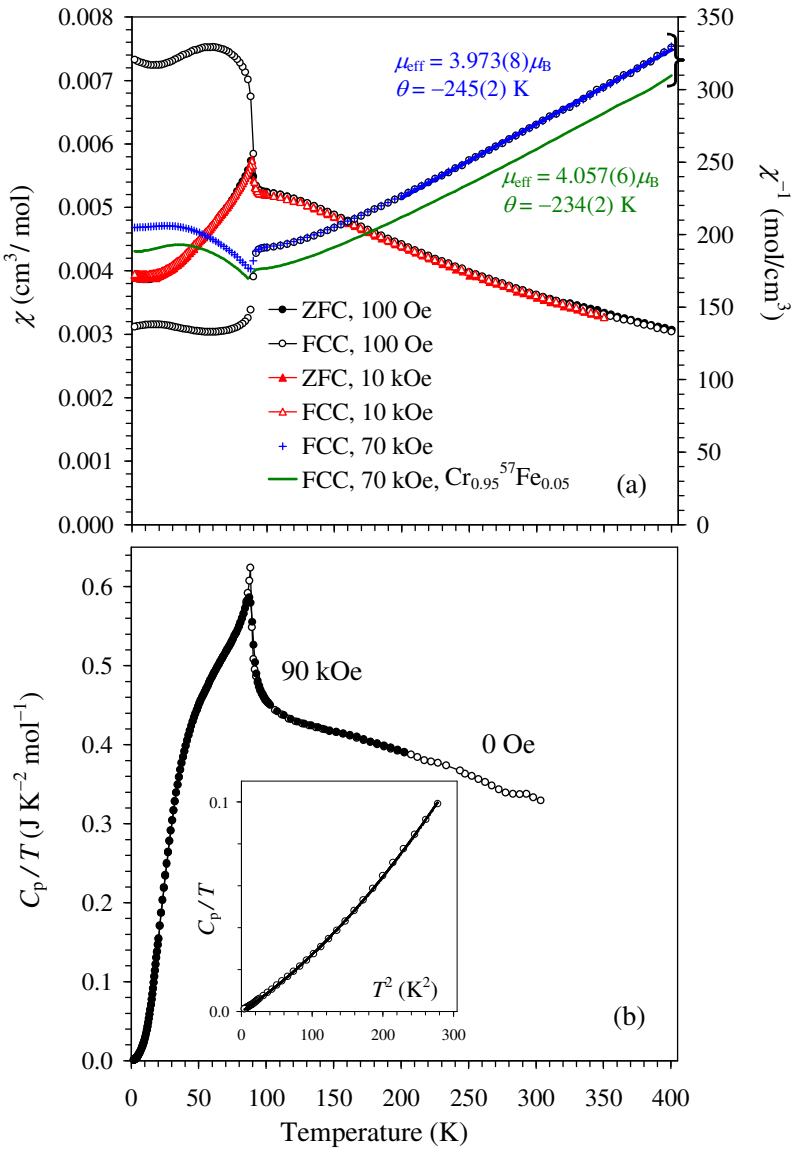

Figure 3. (a: the left-hand axis) ZFC (filled symbols) and FCC (white symbols) dc magnetic susceptibility (χ = M/H) curves of $TlCrO_3$ at 100 Oe and 10 kOe. (a: the right-hand axis) FCC inverse curves (χ^{-1} vs T) of $TlCrO_3$ at 100 Oe and 70 kOe and $TlCr_{0.95}{}^{57}Fe_{0.05}O_3$ at 70 kOe. The parameters (μ_{eff} and θ) of the Curie-Weiss fit between 200 and 400 K are given. (b) Specific heat data of $TlCrO_3$ at a zero magnetic field (white circles) and 90 kOe (black circles) plotted as C_p/T vs T. The inset shows the C_p/T vs T^2 curve (symbols) between 2 and 17 K with fitting results (line).

Dalton Transactions Accepted Manuscript

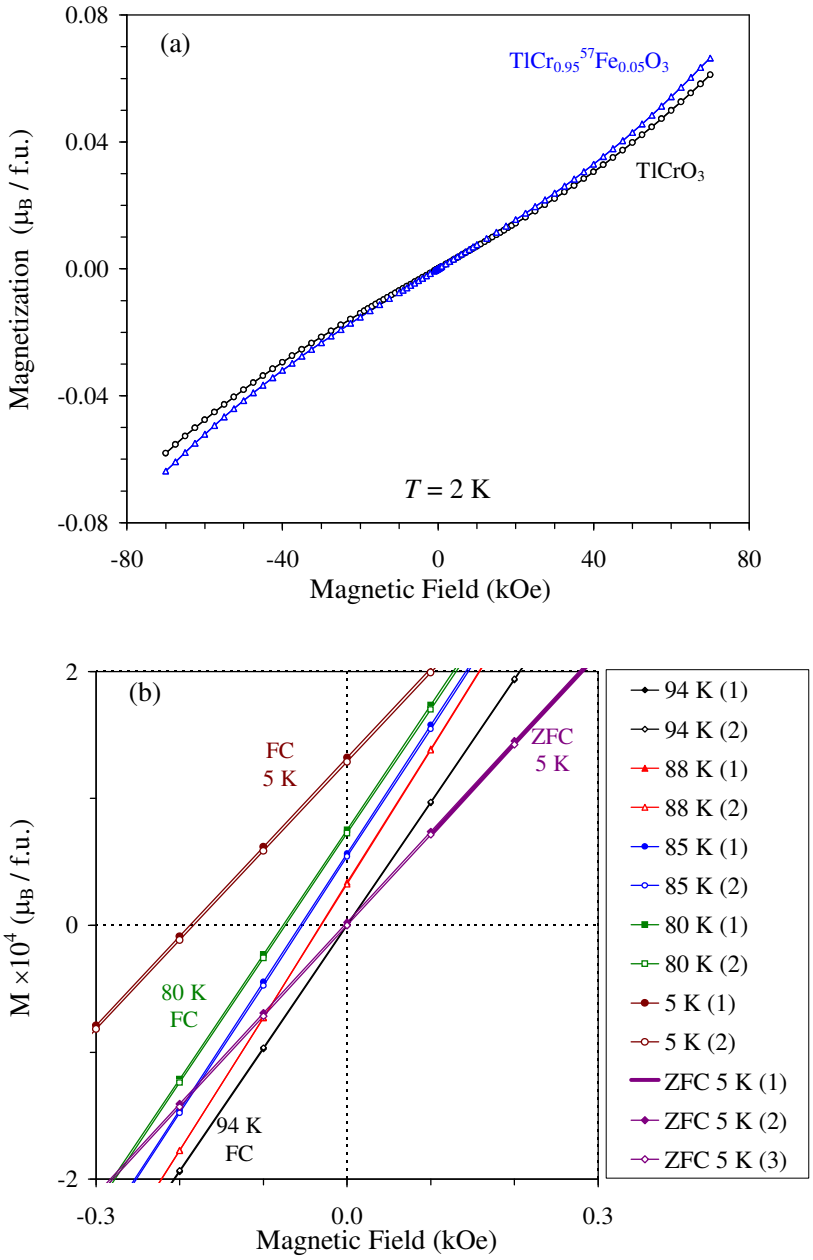

Figure 4. (a) M vs H curves of $TlCrO_3$ and $TlCr_{0.95}{}^{57}Fe_{0.05}O_3$ at 2 K. (b) FC M vs H curves of $TlCrO_3$ at 5, 80, 85, 88 and 94 K and ZFC M vs H curves at 5 K. Details between –0.3 and 0.3 kOe are shown; the M v H curves themselves were measured between –10 and 10 kOe. For FC, (1) is the branch measured from 10 kOe to –10 kOe and (2) is the branch measured from –10 kOe to 10 kOe. For ZFC, (1) is the branch measured from 100 Oe to 10 kOe, (2) is the branch measured from 10 kOe to –10 kOe and (3) is the branch measured from –10 kOe to 10 kOe.

Dalton Transactions Accepted Manuscript

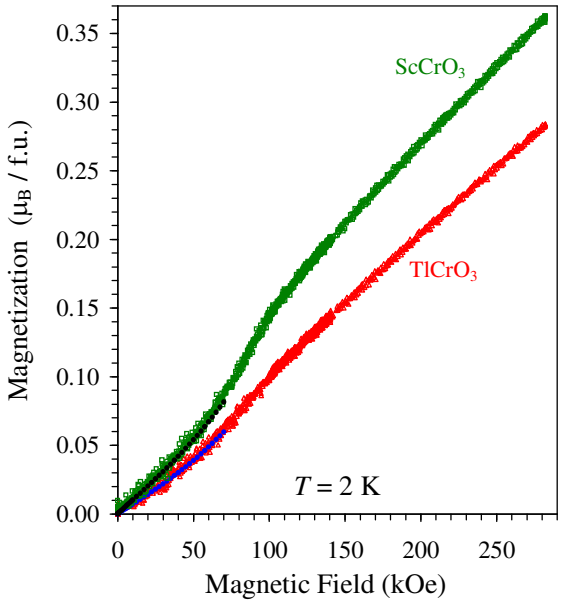

Figure 5. M vs H curves of $TlCrO_3$ and $ScCrO_3$ at 2 K measured with the NIMS hybrid magnet from 0 to 280 kOe and from 280 to 0 kOe. The filled symbols show M vs H curves of $TlCrO_3$ and $ScCrO_3$ at 2 K measured with an MPMS up to 70 kOe.

Dalton Transactions Accepted Manuscript

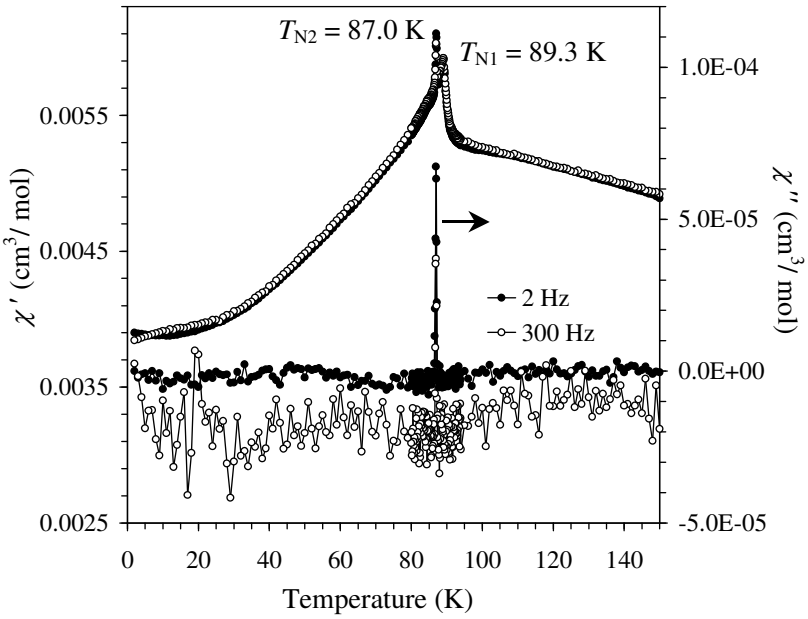

Figure 6. Real χ' (the left-hand axes) and imaginary χ'' (the right-hand axes) parts of the ac susceptibility as a function of temperature (2–150 K) for $TlCrO_3$. Measurements were performed on cooling at a zero static magnetic field using the ac field with the amplitude H_{ac} = 5 Oe and frequencies f = 2 and 300 Hz.

Dalton Transactions Accepted Manuscript

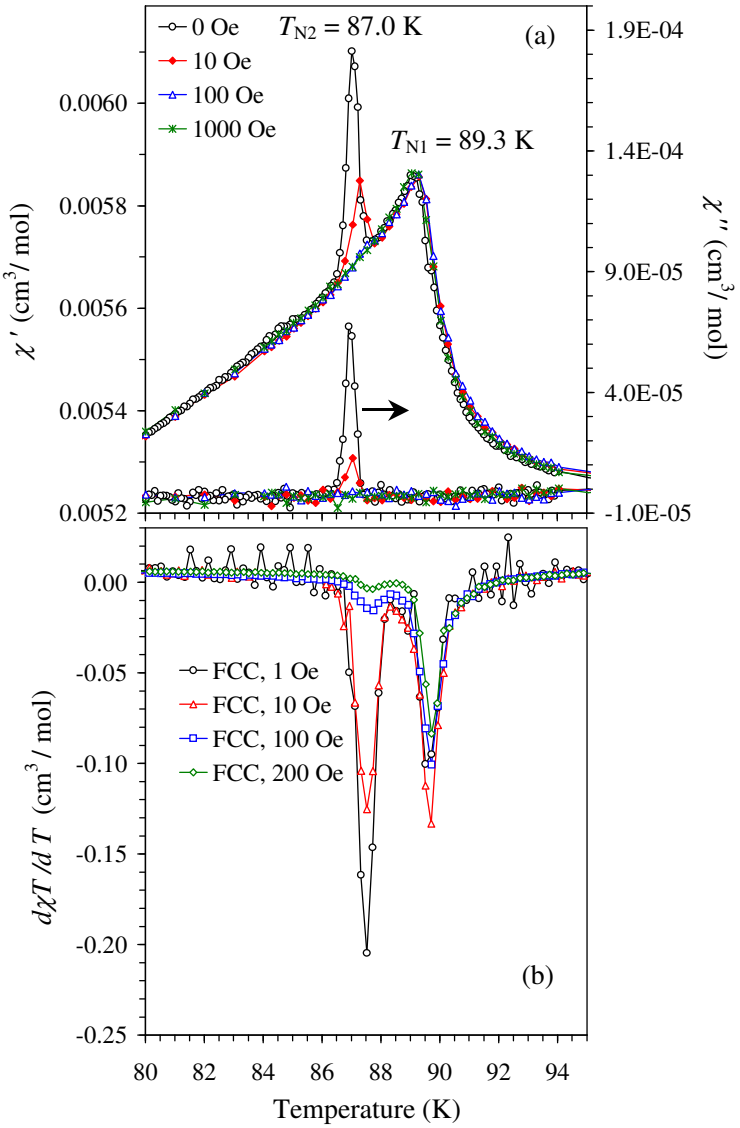

Figure 7. (a) Real χ' (the left-hand axes) and imaginary χ'' (the right-hand axes) parts of the ac susceptibilities of $TlCrO_3$ (H_{ac} = 5 Oe and f = 2 Hz) at static magnetic fields of 0, 10, 100 and 1000 Oe. (b) dc FCC $d\chi T/dT$ vs T curves of $TlCrO_3$ at different magnetic fields with a fine step of 0.2 K.

Dalton Transactions Accepted Manuscript

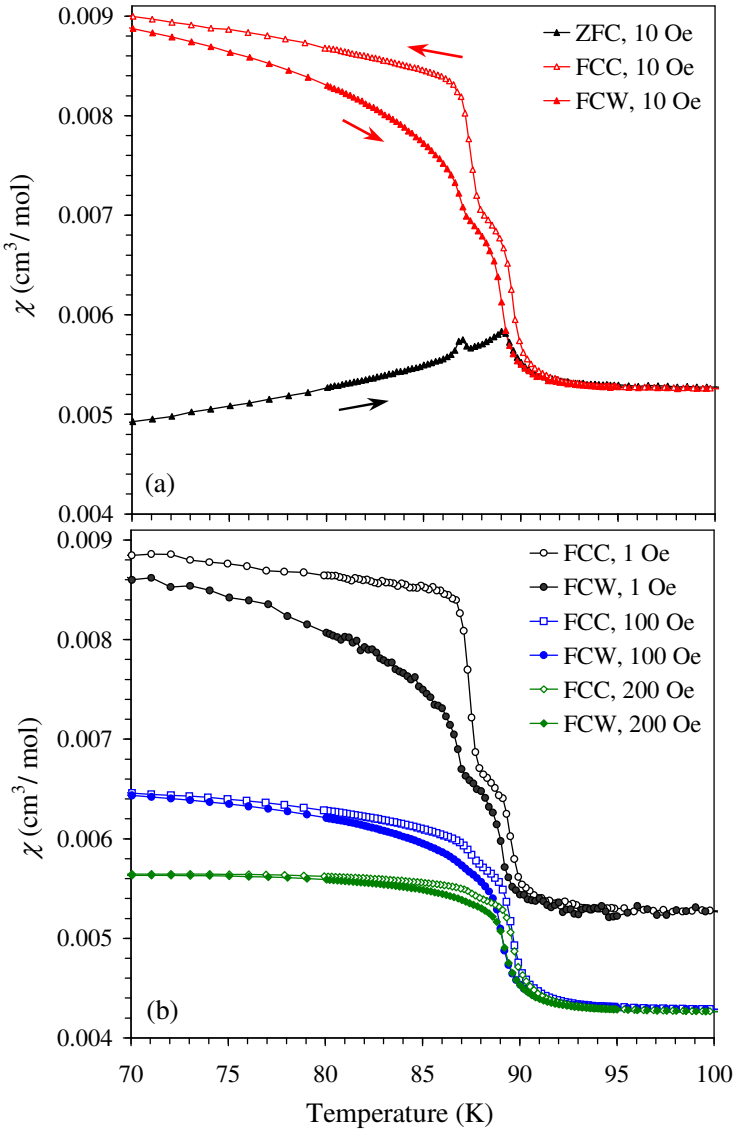

Figure 8. ZFC, FCC and FCW dc magnetic susceptibility curves of $TlCrO_3$ at 10 Oe with a fine measurement step of 0.2 K near T_N. (b) FCC and FCW dc magnetic susceptibility curves of $TlCrO_3$ at 1, 100 and 200 Oe. The curves at 100 and 200 Oe are shifted by –0.001 cm^3/mol for the clarity.

Dalton Transactions Accepted Manuscript

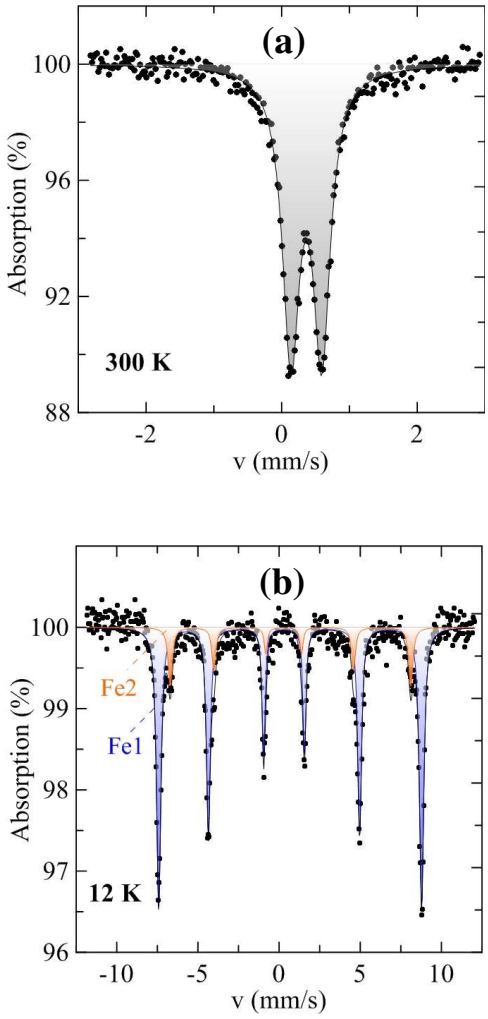

Figure 9. ^{57}Fe Mössbauer spectra of $TlCr_{0.95}{}^{57}Fe_{0.05}O_3$ at (a) 300 K and (b) 12 K (black circles) with fitting results (lines).

Dalton Transactions Accepted Manuscript

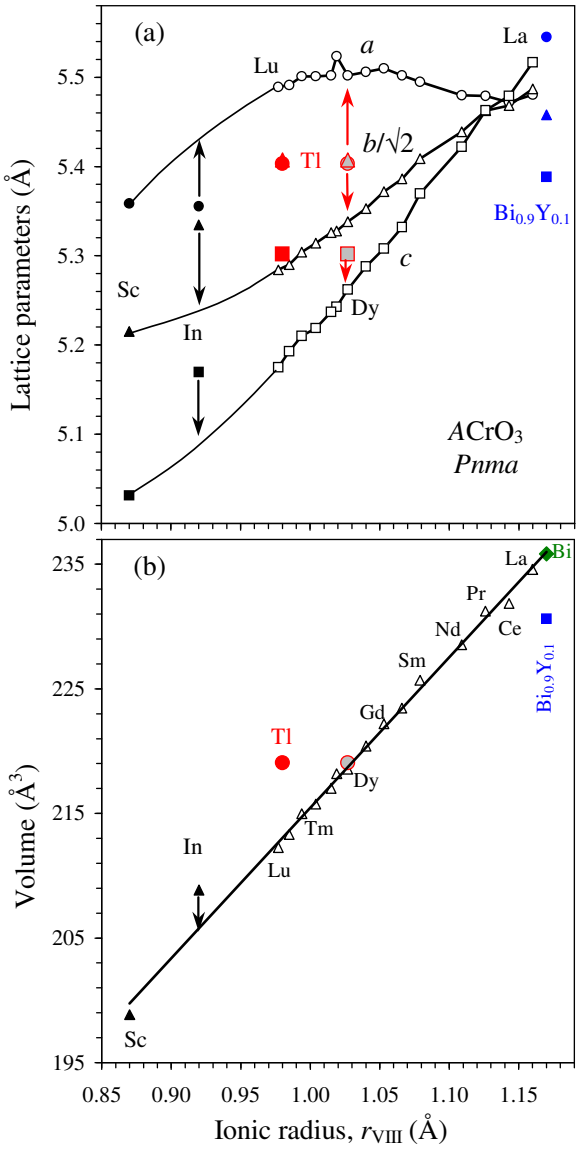

Figure 10. Room-temperature lattice parameters and unit cell volume of ACrO$_3$ compounds (A^{3+} = Sc, In, Tl, Y, rare-earths and Bi$_{0.9}$Y$_{0.1}$)[23] crystallizing in space group *Pnma* as a function of the ionic radius (in the 8-fold coordination).[22] The lines through the lattice parameters are the smooth lines drawn for eye; the solid line through the volumes is the least-square linear fit of the data for RCrO$_3$ (R = La-Lu). BiCrO$_3$ crystallizes in a different space group of $C2/c$; therefore, only the volume is given. Arrows show expected lattice parameters for InCrO$_3$ and TlCrO$_3$ from the monotonic trends in the family. The data for TlCrO$_3$ are given with two ionic radii, $r_{VIII}(Tl^{3+})$ = 0.98 Å (the Shannon ionic radius)[22] and $r_{VIII}(Tl^{3+}) = r_{VIII}(Dy^{3+})$ = 1.027 Å.

Dalton Transactions Accepted Manuscript

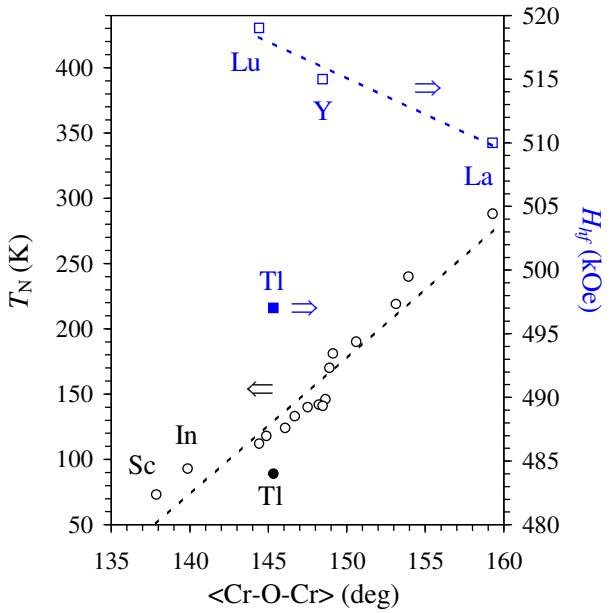

Figure 11. Néel temperatures (T_N)[4,20,49] and hyperfine magnetic fields (H_{hf})[49] at the ^{57}Fe nuclei in ACrO$_3$ (A = Sc, In and Lu-La) and TlCrO$_3$ as a function of the average Cr-O-Cr bond angle (experimental values for A = Sc, In,[20] Y[41] and La-Lu[48]).

Dalton Transactions Accepted Manuscript

Figure For Table of Contents Only

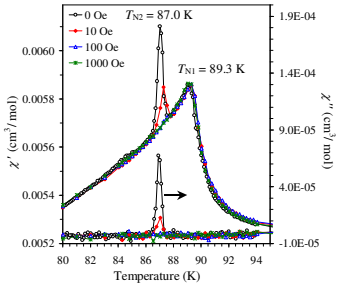

$TlCrO_3$ perovskite has many peculiarities in comparison with $RCrO_3$ (R = rare earths), originating from strong covalency of Tl^{3+}-O bonds.

Dalton Transactions Accepted Manuscript

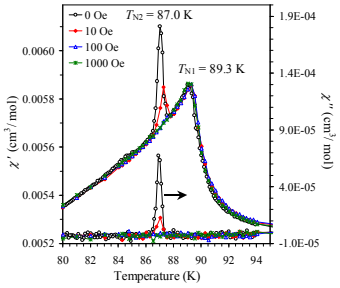

$TlCrO_3$ perovskite has many peculiarities in comparison with $RCrO_3$ (R = rare earths), originating from strong covalency of Tl^{3+}-O bonds.

Dalton Transactions Accepted Manuscript